*As per UGC guidelines an electronic bar code is provided to secure your paper*

*International Journal for Modern Trends in Science and Technology*
*Volume 12, Issue 08*, pages 66-79.
ISSN: 2455-3778 online
Available online at: http://www.ijmtst.com/vol12issue06.html
DOI: https://doi.org/10.5281/zenodo.22151960

# Design and Performance Analysis of an ANFIS-Controlled Grid-Integrated PV Based EV Charging System with SEPIC–Cuk Converter for Power Quality Enhancement

**G. Lokesh Reddy | Dr. S. Munisekhar | Dr. K. Siva Kumar**

*Department of Electrical & Electronics Engineering, Sri Venkatesa Perumal College of Engineering and Technology, Puttur, Andhra Pradesh, India.*

**To Cite this Article**
G. Lokesh Reddy, Dr. S. Munisekhar & Dr. K. Siva Kumar (2026). Design and Performance Analysis of an ANFIS-Controlled Grid-Integrated PV Based EV Charging System with SEPIC–Cuk Converter for Power Quality Enhancement. International Journal for Modern Trends in Science and Technology, 12(08), 66-79. https://doi.org/10.5281/zenodo.22151960

**Article Info**
Received: 28 July 2026; Revised: 16 August 2026; Accepted: 20 July 2026.



*KEYWORDS*

*Adaptive Neuro-Fuzzy Inference System (ANFIS), electric vehicle (EV) charging, photovoltaic (PV) system, grid-connected system, SEPIC–Cuk converter, Shunt Active Power Filter (SAPF), Voltage Source Converter (VSC), power quality, harmonic mitigation.*

**ABSTRACT**

*This paper presents a grid-integrated photovoltaic (PV) based electric vehicle (EV) charging system with enhanced power quality and system stability using an Adaptive Neuro-Fuzzy Inference System (ANFIS) controller. The proposed system utilizes a SEPIC–Cuk DC–DC converter to achieve high voltage gain and efficient power conversion from the PV source for EV battery charging applications. To overcome the limitations of conventional PI based control methods under dynamic operating conditions, an ANFIS based intelligent control strategy is implemented for converter voltage regulation, energy management, and stable power transfer between the PV source, EV battery, and utility grid. In addition, a nonlinear load is connected at the grid side to evaluate the power quality performance under distorted operating conditions. A grid-side voltage source converter (VSC) is employed as a Shunt Active Power Filter (SAPF) to mitigate current harmonics and reactive power disturbances caused by nonlinear loads. The reference compensating currents are generated using the d-q reference current control technique, enabling accurate harmonic extraction and effective current compensation. The proposed control strategy significantly improves grid current quality, reduces Total Harmonic Distortion (THD), and enhances system stability during load and irradiance variations. The complete system is modeled and analyzed using MATLAB Simulink. Simulation results demonstrate improved DC bus voltage regulation, faster dynamic response, enhanced converter efficiency, reduced harmonic distortion, improved power factor, and compliance with Institute of Electrical and Electronics Engineers IEEE-519 power quality standards. The proposed system provides an efficient*

## I. Introduction

The rapid growth of electric vehicles (EVs) has accelerated the global transition toward sustainable transportation and significantly increased the demand for reliable, efficient, and intelligent charging infrastructure. The electrification of transportation is recognized as an effective strategy for reducing greenhouse gas emissions, improving energy security, and decreasing dependence on fossil fuels. However, the increasing penetration of EV charging stations imposes considerable challenges on modern distribution networks, including increased peak demand, voltage fluctuations, harmonic distortion, reactive power consumption, transformer overloading, and deterioration of overall power quality [1], [2]. Consequently, integrating renewable energy sources with EV charging stations has emerged as an attractive solution for reducing grid dependency while promoting environmentally sustainable energy utilization. Such integrated systems not only improve energy efficiency but also contribute to reducing carbon emissions and supporting the development of future smart grids [3], [4]. Among the available renewable energy resources, solar photovoltaic (PV) technology has gained widespread attention because of its abundant availability, modular installation, low operating cost, minimal maintenance requirements, and continuously decreasing installation cost. Grid-connected PV systems can directly supply clean electrical energy to EV charging stations during daylight hours while exchanging surplus or deficit power with the utility grid according to system operating conditions [5], [6]. Nevertheless, the output power of PV systems is highly dependent on solar irradiance and ambient temperature, leading to significant variations in generated power. These fluctuations adversely affect EV charging performance, DC-link voltage regulation, converter stability, and overall system reliability under dynamic environmental conditions [7], [8]. Therefore, efficient power electronic converters and intelligent control algorithms are essential for maintaining stable operation and ensuring uninterrupted power transfer between the PV source, EV battery, and utility grid. High-gain DC–DC converters play an important role in renewable-energy-based EV charging systems by providing efficient voltage conversion and regulating power flow from the PV array to the battery charging unit. Conventional boost converters require extremely high duty cycles to achieve large voltage gains, which increases switching losses, voltage stress across semiconductor devices, current ripple, and overall system inefficiency [9]. To overcome these limitations, hybrid converter topologies have been extensively investigated in recent years. Among them, the combination of Single-Ended Primary Inductor Converter (SEPIC) and Cuk converter offers several advantages, including high voltage conversion ratio, continuous input current, reduced output current ripple, improved voltage regulation, lower switching stress, and enhanced conversion efficiency over a wide operating range [10], [11]. Owing to these desirable characteristics, the SEPIC–Cuk converter is highly suitable for photovoltaic-based EV charging applications requiring stable and efficient power conversion. The overall performance of renewable energy conversion systems depends significantly on the effectiveness of the employed control strategy. Conventional proportional-integral (PI) controllers are widely used because of their simple implementation, low computational complexity, and satisfactory steady-state performance. However, their performance deteriorates under nonlinear operating conditions, parameter uncertainties, rapid irradiance variations, sudden load disturbances, and changes in battery charging conditions. Furthermore, PI controllers require precise mathematical models and fixed controller gains, making them less suitable for highly dynamic renewable energy applications [12], [13]. Consequently, artificial intelligence (AI)-based control techniques have gained considerable research interest because of their capability to handle nonlinearities, uncertainties, and continuously changing operating conditions. Among various intelligent control approaches, the Adaptive Neuro-Fuzzy Inference System (ANFIS) has emerged as one of the most promising techniques for renewable energy applications. ANFIS combines the human reasoning capability of fuzzy logic with the adaptive learning characteristics of artificial neural networks, thereby providing accurate nonlinear mapping, self-learning capability, adaptive parameter tuning, and robust control performance [14], [15]. Unlike conventional fuzzy logic controllers that require manual selection of membership functions and rule parameters, ANFIS automatically adjusts these parameters using training data, resulting in improved control accuracy and reduced steady-state error [16]. Several researchers have reported that ANFIS-based controllers exhibit faster transient response, superior voltage regulation, better disturbance rejection, and enhanced robustness compared with conventional PI and standalone fuzzy logic controllers under varying operating conditions [17], [18]. These advantages make ANFIS particularly suitable for controlling high-performance PV-fed EV charging systems operating under continuously changing environmental and loading conditions. In addition to efficient converter control, maintaining acceptable power quality has become one of the major challenges in grid-connected renewable energy systems because of the widespread utilization of nonlinear loads and power electronic converters. Nonlinear loads inject harmonic currents into the utility grid, leading to increased Total Harmonic Distortion (THD), poor power factor, excessive neutral currents, transformer overheating, additional power losses, and reduced lifetime of electrical equipment [19], [20]. To ensure reliable and efficient power system operation, international standards such as IEEE Std. 519 specify permissible harmonic limits and recommend suitable harmonic mitigation techniques for grid-connected installations [21]. Therefore, effective harmonic compensation methods are indispensable for renewable-energy-based EV charging infrastructures. Among the available power quality improvement techniques, Shunt Active Power Filters (SAPFs) have become one of the most effective solutions for mitigating current harmonics and compensating reactive power. A Voltage Source Converter (VSC)-based SAPF injects compensating currents equal in magnitude and opposite in phase to the harmonic currents produced by nonlinear loads, thereby restoring sinusoidal grid currents and improving the overall power factor [22], [23]. The performance of SAPFs largely depends on the accuracy of reference current generation. Among various control techniques, the synchronous reference frame (SRF) or d–q reference current control method has been widely adopted because of its excellent harmonic extraction capability, fast dynamic response, simple implementation, and effective compensation under both balanced and unbalanced operating conditions [24], [25]. Consequently, integrating SAPF functionality into renewable-energy-based EV charging systems significantly enhances grid current quality and ensures compliance with power quality standards [26]. Recently, considerable research has been devoted to intelligent control strategies for PV-based EV charging systems. Existing studies have investigated various converter topologies, maximum power point tracking algorithms, battery management techniques, and advanced control methods for improving charging efficiency and renewable energy utilization. Nevertheless, many reported works primarily focus on converter performance or charging management individually, while comparatively less attention has been given to the simultaneous improvement of converter efficiency, intelligent energy management, harmonic mitigation, reactive power compensation, and grid power quality under nonlinear loading conditions [27]. Moreover, recent advancements in electric vehicle technology have emphasized bidirectional charging capability, smart energy management, vehicle-to-grid operation, and coordinated interaction between EV charging stations and utility grids for improving overall system flexibility and reliability [28], [29]. In parallel, continuous developments in modern power electronic converters and intelligent digital control techniques have enabled higher conversion efficiency, improved reliability, reduced switching losses, and superior dynamic performance in renewable energy systems [30]. These advancements highlight the necessity for integrated intelligent control strategies capable of simultaneously addressing renewable energy utilization, EV charging performance, and grid power quality enhancement. Motivated by these research challenges, this paper proposes an ANFIS-controlled grid-integrated photovoltaic-based EV charging system employing a high-gain SEPIC–Cuk DC–DC converter and a grid-side Voltage Source Converter operating as a Shunt Active Power Filter. The proposed ANFIS controller performs intelligent converter voltage regulation and energy management while ensuring stable power transfer among the photovoltaic source, EV battery, and utility grid under varying irradiance and load conditions. Simultaneously, the SAPF employs the synchronous reference frame-based d–q current control technique to generate accurate compensating currents for mitigating harmonics and reactive power introduced by nonlinear loads connected to the grid. The entire system is modeled and validated in the MATLAB/Simulink environment under different operating scenarios. Simulation results demonstrate significant improvements in DC-link voltage regulation, converter efficiency, transient response, EV charging performance, grid current quality, harmonic compensation, power factor, and overall system stability. Furthermore, the proposed system successfully satisfies the harmonic limits specified by IEEE Std. 519, demonstrating its suitability as an efficient and intelligent solution for next-generation renewable-energy-based EV charging infrastructure.

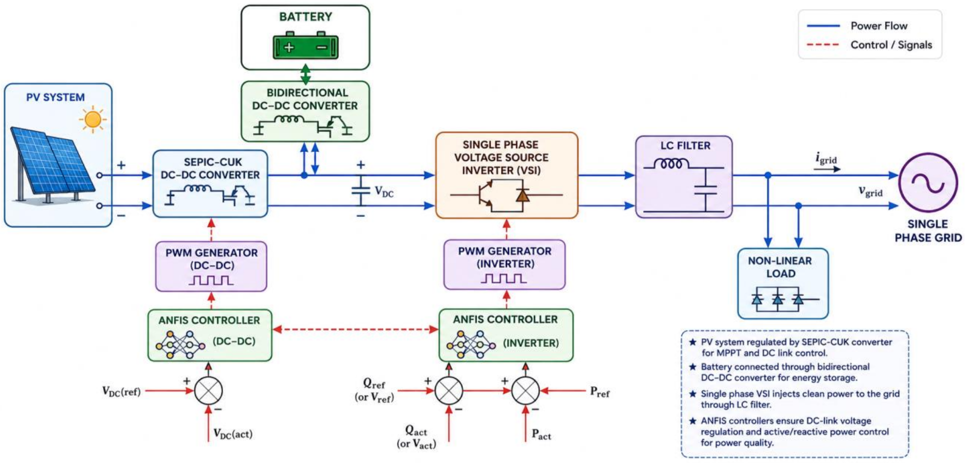


Fig. 1. Proposed ANFIS-controlled grid-integrated PV-based EV charging system with SEPIC–Cuk converter

## II. System Configuration

Fig. 1 illustrates the proposed ANFIS-controlled grid-integrated PV-based EV charging system. A photovoltaic (PV) array supplies renewable power to a high-gain SEPIC–Cuk DC–DC converter, which performs Maximum Power Point Tracking (MPPT) and regulates the DC-link voltage. A bidirectional DC–DC converter connects the EV battery to the DC bus, enabling charging and discharging operations for efficient energy management. The regulated DC power is converted into AC power by a single-phase Voltage Source Inverter (VSI) and injected into the utility grid through an LC filter. A nonlinear load is connected at the Point of Common Coupling (PCC) to evaluate the power quality performance. The grid-side VSI operates as a Shunt Active Power Filter (SAPF), compensating harmonic currents and reactive power using the synchronous reference frame (d–q) control method. Two ANFIS controllers are employed to improve system performance. The first controller regulates the SEPIC–Cuk converter by maintaining the DC-link voltage, while the second controller controls the inverter to ensure stable active and reactive power exchange with the grid. The proposed system provides efficient EV charging, stable DC-link voltage, improved power factor, reduced Total Harmonic Distortion (THD), and compliance with IEEE Std. 519 power quality standards.

## III. Modeling of the PV System

The photovoltaic (PV) array is the primary renewable energy source in the proposed EV charging system. It converts solar irradiance into electrical energy through the photovoltaic effect. The electrical behavior of the PV module is represented by the single-diode equivalent circuit shown in Fig. 2, which consists of a photocurrent source Iph, a diode D, a series resistance Rs, and a shunt resistance Rp. The series resistance represents the internal conduction losses, whereas the shunt resistance accounts for the leakage current within the PV cell.

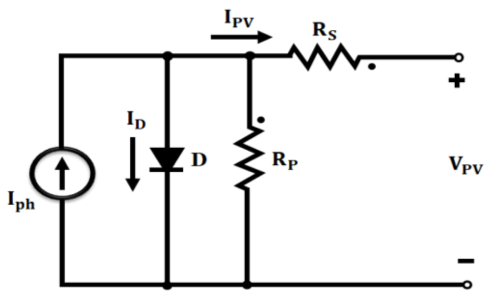


Fig. 2. Single-diode equivalent circuit of the photovoltaic (PV) module.

The output current of the PV module is obtained by applying Kirchhoff's current law to the equivalent circuit and is expressed as

$$I_{Pv} = I_{Ph} - I_D - I_{sh} \quad (1)$$

where IPV is the output current, ID is the diode current, and Ish is the shunt leakage current.

According to the Shockley diode equation, the diode current is given by

$$I_D = I_0 \left[exp\left(\frac{q(V_{pv}+I_{pv}R_s)}{AkT}\right) - 1\right] \quad (2)$$

where Io is the reverse saturation current, q is the electron charge (1.602×10−19C), A is the diode ideality factor, k is Boltzmann's constant (1.381×10−23J/K), and T is the cell temperature in Kelvin.

The shunt current flowing through the parallel resistance is expressed as

$$I_{sh} = \frac{V_{Pv}+I_{Pv}R_S}{R_P} \quad (3)$$

Substituting (2) and (3) into (1), the complete current–voltage characteristic of the PV module becomes

$$I_{Pv} = I_{Ph} - I_0 \left[exp\left(\frac{q(V_{pv}+I_{pv}R_s)}{AkT}\right) - 1\right] - \frac{V_{Pv}+I_{Pv}R_S}{R_P} \quad (4)$$

The photocurrent generated by the PV module depends on the solar irradiance and operating temperature and is calculated as

$$I_{Ph} = [I_{sc} + K_i(T - T_{ref})]\frac{G}{Gref} \quad (5)$$

where $I_{sc}$ is the short-circuit current, $K_i$ is the temperature coefficient of current, G is the incident solar irradiance, and $G_{ref}$ is the reference irradiance under standard test conditions.

The output power of the PV array is obtained as

$$P_{PV} = V_{PV}I_{PV} \quad (6)$$

The generated PV power varies continuously with changes in solar irradiance and cell temperature. Therefore, a high-gain SEPIC–Cuk converter is employed to extract the maximum available power from the PV array while maintaining a regulated DC-link voltage. The proposed ANFIS controller continuously adjusts the converter duty ratio according to the DC-link voltage error, thereby improving power extraction efficiency, voltage regulation, and overall system stability under dynamic operating conditions.

## IV. Modeling and Design of the SEPIC–Cuk DC–DC Converter

The proposed EV charging system employs a high-gain SEPIC–Cuk DC–DC converter to regulate the photovoltaic output voltage and maintain a constant DC-link voltage under varying solar irradiance conditions. The converter combines the advantages of the Single-Ended Primary Inductor Converter (SEPIC) and the Ćuk converter to achieve a high voltage conversion ratio, continuous input current, low output current ripple, and improved conversion efficiency. Furthermore, the converter provides better voltage regulation with reduced switching stress, making it suitable for renewable energy-based EV charging applications. The circuit configuration of the proposed SEPIC–Cuk converter is illustrated in Fig. 3.

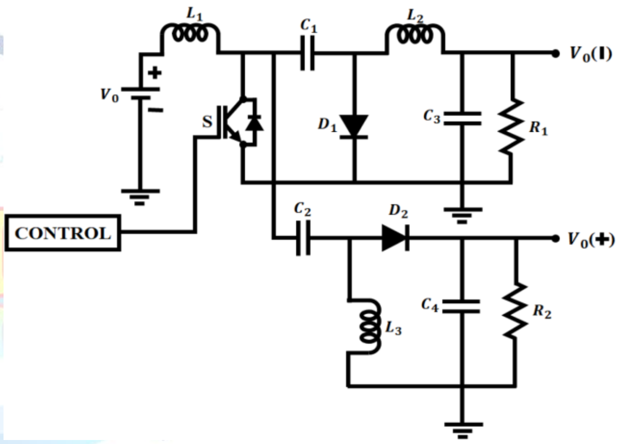


Fig. 3. Circuit configuration of the proposed SEPIC–Cuk DC–DC converter.

The converter operates in two switching modes depending on the state of switch S.

Mode I (Switch ON)

When switch S is turned ON, diode D1 becomes reverse biased while diode D2 remains forward biased. During this interval, inductors L1 and L3 store energy from the photovoltaic source, whereas capacitor C1 transfers energy to the load through inductor L2. The voltage across the inductors can be expressed as

$$V_{L1} = V_{PV}$$
$$V_{L2} = V_{C1} - V_0 \quad (7)$$
$$V_{L3} - V_{C2}$$

The inductor currents increase linearly according to

where $V_L$ represents the corresponding inductor voltage.

Mode II (Switch OFF)

When switch S is turned OFF, diode D1 becomes forward biased and transfers the stored energy from inductors L1 and L3 to the output. Simultaneously, capacitor C1 is recharged, and the output capacitor maintains a constant load voltage. The inductor voltages during this interval are given by

$$V_{L1} = V_{PV} - V_{C1}$$
$$V_{L2} = -V_0 \qquad (8)$$
$$V_{L3} = V_{C2} - V_0$$

Applying the volt-second balance principle to the inductors under continuous conduction mode (CCM), the steady-state voltage conversion ratio of the SEPIC–Cuk converter is obtained as

$$\frac{V_0}{V_{PV}} = \frac{D}{1-D} \qquad (9)$$

where D denotes the duty cycle of the switching device.

The inductance required for continuous conduction mode is determined by

$$L = \frac{V_{PV}D}{\Delta I_L f_S} \qquad (10)$$

where fs is the switching frequency and ΔIL is the allowable inductor current ripple.

The energy transfer capacitor is selected as

$$C = \frac{I_0 D}{\Delta V_C f_S} \qquad (11)$$

where Io is the output current and $\Delta V_C$ represents the capacitor voltage ripple.

Similarly, the output filter capacitor is calculated as

$$C_0 = \frac{I_0 D}{\Delta V_0 f_S} \qquad (12)$$

where $\Delta V_0$ denotes the permissible output voltage ripple.

The output power delivered by the converter is expressed as

$$P_o = V_o I_o \qquad (13)$$

To achieve accurate voltage regulation, an ANFIS controller continuously monitors the DC-link voltage error and generates the optimal PWM duty ratio for switch S. The adaptive learning capability of the ANFIS controller enables rapid tracking of photovoltaic power variations, improved transient response, and stable DC-link voltage regulation under dynamic irradiance and load conditions. Consequently, the proposed SEPIC–Cuk converter provides efficient power conversion, reduced switching losses, enhanced voltage gain, and improved overall system efficiency.

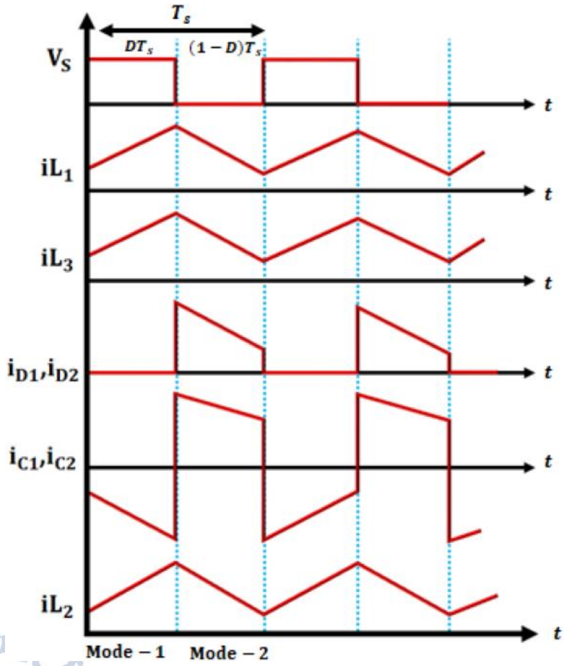


Fig. 4. Waveform of SEPIC–Cuk converter

### V. Modeling and Design of the Single-Phase Voltage Source Inverter

The regulated DC power obtained from the SEPIC–Cuk converter is converted into AC power using a single-phase Voltage Source Inverter (VSI) for grid integration, as shown in Fig. 5. The inverter injects the generated active power into the utility grid while maintaining synchronization with the grid voltage. A sinusoidal Pulse Width Modulation (SPWM) technique is employed to generate the switching pulses for the inverter. The PWM pulses are obtained from the controller based on the active power error, ensuring stable power transfer and improved dynamic performance.

The output voltage of the single-phase VSI is expressed as

$$V_{inv} = mV_{dc}$$

where Vdc is the DC-link voltage and m is the modulation index.

The instantaneous output power supplied to the grid is

$$p = V_{grid} I_{grid} \cos \phi \qquad (14)$$

where $V_{grid}$ and $I_{grid}$ are the grid voltage and current, respectively, and ϕ is the phase angle between them.

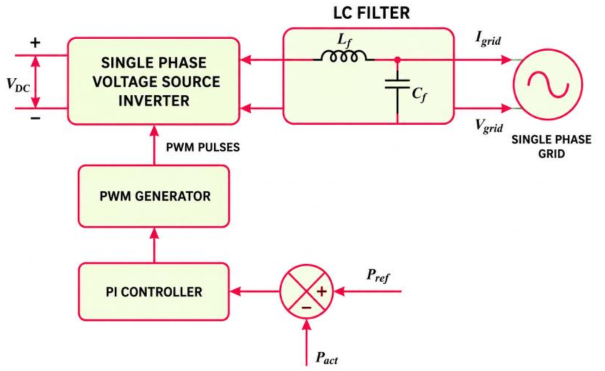


Fig. 5. Single-phase voltage source inverter with LC filters and power control for grid integration.

The controller regulates the inverter output by minimizing the active power error given by

$$e_P = P_{ref} - P_{act} \quad (15)$$

where Pref is the reference active power and Pact is the measured active power.

The control signal generated by the controller is represented as

$$u(t) = K_p e_P + K_i \int e_P \, dt \quad (16)$$

where $K_p$ and $K_i$ denote the proportional and integral gains, respectively. The controller output is supplied to the PWM generator, which produces the switching pulses for the VSI.

LC Filter Design

An LC filter is connected between the inverter and the utility grid to suppress high-frequency switching harmonics and improve the quality of the injected grid current. The filter inductance is determined by

$$L_f = \frac{V_{dc}}{8 f_s \Delta I} \quad (17)$$

where $f_s$ is the switching frequency and ΔI is the allowable current ripple.

The filter capacitance is calculated as

$$C_f = \frac{1}{(2\pi f_C)^2 L_f} \quad (18)$$

where $f_C$ is the filter cut-off frequency.

The resonant frequency of the LC filter is given by

$$f_r = \frac{1}{2\pi\sqrt{L_f C_f}} \quad (19)$$

The LC filter effectively attenuates switching-frequency harmonics while allowing the fundamental frequency component to pass with negligible attenuation. Consequently, the injected grid current becomes nearly sinusoidal, resulting in lower Total Harmonic Distortion (THD) and improved power quality. In the proposed system, the inverter controller continuously compares the reference active power with the measured grid power and adjusts the PWM modulation index accordingly. This control strategy enables stable DC-link voltage regulation, accurate active power injection, fast transient response, and improved power factor during dynamic operating conditions. The integration of the LC filter further enhances the quality of the injected current, ensuring compliance with the IEEE Std. 519 harmonic limits.

## VI. Modeling and Operation of the Bidirectional DC–DC Converter

The bidirectional DC–DC converter provides an interface between the DC-link and the battery energy storage system (BESS), enabling bidirectional power flow for charging and discharging operations. It improves the stability of the DC-link voltage by storing excess photovoltaic energy during high irradiance conditions and supplying the stored energy during low irradiance or high load demand. Consequently, the battery enhances the reliability and uninterrupted operation of the grid-integrated PV-based EV charging system. The circuit configuration of the bidirectional DC–DC converter is shown in Fig. 6.

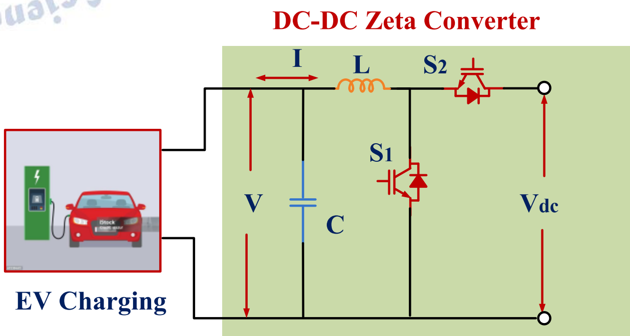


Fig. 6. Bidirectional DC–DC converter for battery charging and discharging operations.

The converter consists of two controlled switches (S1 and S2), an inductor L, and capacitors connected across the DC-link and battery terminals. Depending on the power balance between the PV source and the load demand, the converter operates either in charging mode or discharging mode.

1) Charging Mode

When the photovoltaic power exceeds the load demand, the battery is charged through buck converter operation. In this mode, switch S1 is modulated while switch S2 remains OFF. The DC-link supplies power to the battery through the inductor.

The inductor voltage during charging is expressed as

$$V_L = V_{dc} - V_{batt} \quad (20)$$

The battery charging current is

$$L\frac{dI_{batt}}{dt} = V_{dc} - V_{batt} \quad (21)$$

The battery charging power is

$$P_{ch} = V_{batt}I_{batt} \quad (22)$$

The output voltage of the converter during charging is

$$V_{batt} = DV_{dc} \quad (23)$$

where D denotes the PWM duty ratio.

2) Discharging Mode

During insufficient photovoltaic generation or sudden load variations, the battery operates in boost mode and supplies power to the DC-link. In this operating mode, switch S2 is modulated while switch S1 remains OFF.

The inductor voltage is

$$V_L = V_{batt} \quad (25)$$

The battery current is governed by

$$L\frac{dI_{batt}}{dt} = V_{batt} \quad (26)$$

The boosted DC-link voltage is obtained as

$$V_{dc} = \frac{V_{batt}}{1-D} \quad (27)$$

The battery discharging power is

$$P_{dis} = V_{batt}I_{batt}$$

3) Battery State of Charge

The battery State of Charge (SOC) is continuously monitored to ensure safe charging and discharging operation. The SOC is estimated using the Coulomb counting method as

$$SOC(t) = SOC_0 - \frac{1}{Q_{bat}}\int_0^t I_{batt}(\tau)\,d\tau \quad (28)$$

where

- $SOC_0$ is the initial state of charge,
- $Q_{bat}$ is the battery capacity (Ah),
- $I_{batt}$ is positive during discharge and negative during charging.

The battery terminal power is

$$P_{bat} = V_{batt}I_{batt} \quad (29)$$

The energy stored in the battery is

$$E_{bat} = SOC \times E_{rated} \quad (30)$$

where Erated is the rated battery energy.

4) Working Operation

The proposed bidirectional DC–DC converter automatically switches between charging and discharging modes according to the available PV power and DC-link voltage. When the PV array generates surplus energy, the converter operates in buck mode and charges the battery while maintaining the reference DC-link voltage. Conversely, during low solar irradiance or increased load demand, the converter changes to boost mode and supplies the stored battery energy to the DC-link, thereby supporting continuous EV charging and grid operation. The battery charging and discharging processes are coordinated by the proposed ANFIS controller, which regulates the converter duty ratio based on the DC-link voltage error and battery operating conditions. This intelligent control strategy improves energy utilization, enhances DC-link voltage stability, reduces transient fluctuations, and increases the overall efficiency of the renewable energy-based EV charging system.

## VII. Chaotic Dragonfly Optimization Algorithm (CDAO)

The Chaotic Dragonfly Optimization Algorithm (CDAO) is employed to optimize the parameters of the proposed ANFIS controller, thereby improving the dynamic performance and convergence characteristics of the PV-based EV charging system as shown in Fig. 7. CDAO is an enhanced version of the conventional Dragonfly Algorithm (DA), where chaotic mapping is incorporated to improve population diversity and avoid premature convergence toward local optima. The algorithm imitates the static and dynamic swarming behavior of dragonflies during hunting and migration. By integrating chaotic sequences into the search process, the proposed optimization method achieves faster convergence, better exploration capability, and improved global optimization performance.

The movement of each dragonfly is governed by five social interaction behaviors, namely separation, alignment, cohesion, attraction towards the food source, and distraction from the enemy. The position update of each dragonfly is expressed as

$$\Delta X_{t+1} = (sS + aA + cC + fF + eE) + w\Delta X_t \qquad (31)$$

where

- S = Separation vector
- A = Alignment vector
- C = Cohesion vector
- F = Food attraction vector
- E = Enemy distraction vector
- s,a,c,f,e = corresponding weighting coefficients
- w = inertia weight.

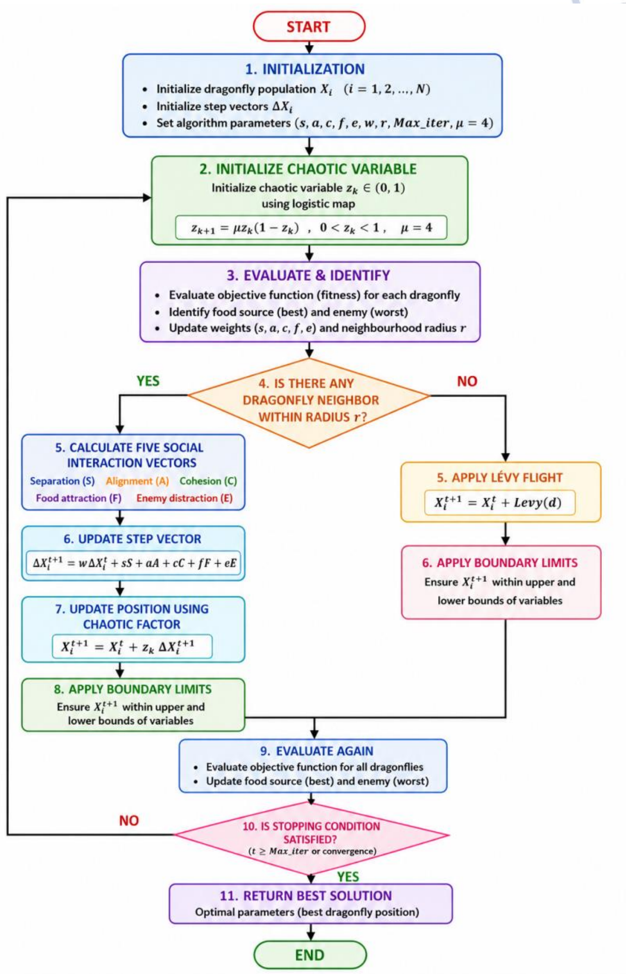


Fig. 7. Flowchart of the Chaotic Dragonfly Optimization Algorithm (CDAO).

The dragonfly position is updated according to

$$X_{t+1} = X_t + \Delta X_{t+1} \qquad (32)$$

where Xt represents the current position of the dragonfly.

Chaotic Search Strategy

To enhance the global searching capability, the logistic chaotic map is incorporated into the dragonfly optimization process. The chaotic variable is generated as

$$z_{k+1} = \mu z_k(1 - z_k) \qquad (33)$$

Where

$0 < z_k < 1$

And

$\mu = 4$

which ensures completely chaotic behavior.

The chaotic factor is introduced into the position updating equation as

$$X_{t+1} = X_t + z_k \Delta X_{t+1} \qquad (34)$$

thereby improving exploration and preventing premature convergence.

When no neighboring dragonflies exist, the search agent performs a Lévy flight to enhance exploration of the search space. The position update is expressed as

$$X_{t+1=X_t+Levy}(d) \qquad (35)$$

where the Lévy flight function is given by

$$Levy(d) = 0.01 \frac{r_1\sigma}{|r_2|^1}/\beta \qquad (36)$$

where r1 and r2 are uniformly distributed random numbers, β=1.5, and

$$\sigma = \left[\frac{\Gamma(1+\beta)\sin(\pi^{\beta}/2)}{\Gamma((1+\beta)/2)\beta 2^{(\beta-1)/2}}\right]^{1/\beta} \qquad (37)$$

where Γ(·) denotes the Gamma function.

The optimization objective is to minimize the ANFIS training error, defined as

where yi is the desired output, y^i is the ANFIS output, and N is the total number of training samples.

The optimal solution obtained by the CDAO algorithm is used to update the ANFIS membership function parameters and consequent parameters, thereby improving controller accuracy and voltage regulation performance.

Algorithm 1: Chaotic Dragonfly Optimization Algorithm

Step 1: Initialize the dragonfly population Xi, step vectors ΔXi, and algorithm parameters.

Step 2: Initialize the chaotic variable using the logistic map.

Step 3: Evaluate the fitness value of each dragonfly according to the objective function.

Step 4: Identify the best solution (food source) and the worst solution (enemy).

Step 5: Calculate the separation, alignment, cohesion, food attraction, and enemy distraction vectors.

Step 6: Update the step vector using (36).

Step 7: Update the dragonfly position using the chaotic factor according to (39).

Step 8: If no neighboring dragonflies exist, perform Lévy flight using (40).

Step 9: Apply boundary constraints and evaluate the updated fitness values.

Step 10: Repeat Steps 3–9 until the maximum number of iterations or convergence criterion is satisfied.

Step 11: Return the optimal ANFIS parameters corresponding to the minimum objective function.

The proposed CDAO algorithm effectively improves the convergence speed and optimization accuracy of the ANFIS controller by maintaining a proper balance between exploration and exploitation during the optimization process. Consequently, the optimized ANFIS controller provides superior DC-link voltage regulation, reduced steady-state error, faster transient response, and improved power quality compared with conventional optimization techniques.

## VIII. ANFIS-Based Controller

The proposed Adaptive Neuro-Fuzzy Inference System (ANFIS) controller is employed to regulate the DC-link voltage of the grid-integrated PV-based EV charging system. The controller combines the learning capability of artificial neural networks with the reasoning ability of fuzzy inference systems to achieve accurate voltage regulation under varying solar irradiance and load conditions as shown in Fig. 8. Compared with conventional PI controllers, the ANFIS controller provides faster convergence, improved dynamic response, reduced steady-state error, and enhanced robustness against nonlinear system uncertainties. The controller continuously adjusts the PWM duty cycle of the SEPIC–Cuk converter and the modulation index of the grid-side inverter to maintain stable power transfer between the PV array, EV battery, and utility grid.

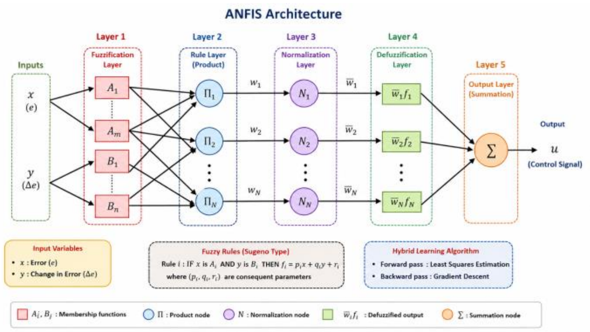


Fig. 8. ANFIS architecture employed for DC-link voltage control in the proposed PV-based EV charging system.

The ANFIS controller receives the DC-link voltage error and the change in voltage error as input variables,

$$e(k) = V_{dc}^{ref} - V_{dc}^{act} \quad (38)$$

$$\Delta e(k) = e(k) - e(k-1) \quad (39)$$

where Vdcref is the reference DC-link voltage and Vdcact is the measured DC-link voltage.

The controller output is expressed as

$$u(k) = f\big(e(k), \Delta e(k)\big) \quad (40)$$

where u(k) represents the control signal used to generate the PWM pulses.

The ANFIS architecture consists of five layers, namely fuzzification, rule evaluation, normalization, defuzzification, and output generation. In the first layer, the input variables are converted into fuzzy membership values using Gaussian membership functions.

$$\mu_i(x) = exp\left[-\frac{(x-c_i)^2}{2\sigma_i^2}\right] \quad (41)$$

where ci and σi denote the center and width of the Gaussian membership function, respectively.

The firing strength of each fuzzy rule is computed as

$$w_i = \mu_A(e)\mu_B(\Delta e) \quad (42)$$

The normalized firing strength is obtained as

$$\overline{w}_i = \frac{w_i}{\sum_{i=1}^{N} w_i} \quad (43)$$

The output of each Sugeno fuzzy rule is represented by

$$f_i = p_{i^e} + q_i \Delta e + r_i \quad (44)$$

where pi, qi, and ri are the consequent parameters.

The final controller output is determined as

$$u = \sum_{i=1}^{N} \bar{\omega}_i f_i \quad (45)$$

The controller parameters are optimized using the hybrid learning algorithm, which combines the least-squares estimation method with gradient descent. The objective function minimized during the training process is

$$E = \frac{1}{2} \sum_{k=1}^{N} (yk - \hat{y}k)^2 \quad (46)$$

where yk denotes the desired output and y^k represents the ANFIS predicted output.

The generated control signal is converted into the PWM duty ratio as

$$D = u(k) \quad (47)$$

which controls the switching operation of the SEPIC–Cuk converter and the grid-side VSI.

Algorithm 1: ANFIS Control Algorithm

Step 1: Initialize the ANFIS structure, Gaussian membership functions, training data, and controller parameters.

Step 2: Measure the DC-link voltage Vdcact.

Step 3: Compute the voltage error

$$e(k) = V_{dc}^{ref} - V_{dc}^{act} \quad (48)$$

and the change in error

$$\Delta e(k) = e(k) - e(k-1) \quad (49)$$

Step 4: Fuzzify the input variables using Gaussian membership functions.

Step 5: Evaluate all fuzzy IF–THEN rules and calculate the firing strengths.

Step 6: Normalize the firing strengths and compute the Sugeno rule outputs.

Step 7: Generate the controller output using the weighted average of all rule outputs.

Step 8: Produce the PWM duty cycle for the SEPIC–Cuk converter and the modulation signal for the grid-side VSI.

Step 9: Update the ANFIS parameters using the hybrid learning algorithm until the error converges.

Step 10: Repeat Steps 2–9 for every sampling interval.

The proposed ANFIS controller continuously adapts its parameters according to the operating conditions, thereby providing accurate DC-link voltage regulation and stable power flow between the PV array, battery energy storage system, and utility grid. Compared with conventional PI controllers, the proposed controller significantly improves transient response, reduces voltage overshoot, minimizes steady-state error, and enhances harmonic compensation under dynamic irradiance and nonlinear loading conditions.

## IX. Simulation Results and Discussion

### *A. Performance Analysis of Grid Voltage, Grid Current, and DC Load Current*

Fig. 9 illustrate the simulated grid voltage, grid current, and DC load current (IL) of the proposed ANFIS-controlled grid-integrated PV-based EV charging system. As shown in Fig. 9 (a), the grid voltage exhibits a stable sinusoidal waveform with a peak amplitude of approximately ±120 V and a constant frequency of 50 Hz, indicating proper synchronization between the single-phase Voltage Source Inverter (VSI) and the utility grid. The corresponding grid current shown in Fig. 9 (b) initially experiences a short transient during converter startup and grid synchronization. However, the transient quickly diminishes, and the current settles into a sinusoidal waveform with a peak value of approximately ±18 A, confirming effective active power injection and near-unity power factor operation. Fig. 9 (c) presents the DC load current (IL), which exhibits an initial overshoot of approximately 35 A due to converter startup and DC-link charging. After the transient period, the current stabilizes at approximately 13 A with very small ripple, demonstrating stable DC power delivery to the EV charging load. The low ripple and steady current confirm the effectiveness of the proposed ANFIS controller in regulating the DC-link voltage and maintaining continuous power flow under varying operating conditions. Overall, the simulation results verify that the proposed control strategy ensures stable grid synchronization, smooth DC load current, improved dynamic response, enhanced power quality, and reliable operation while satisfying the IEEE Std. 519 harmonic requirements.

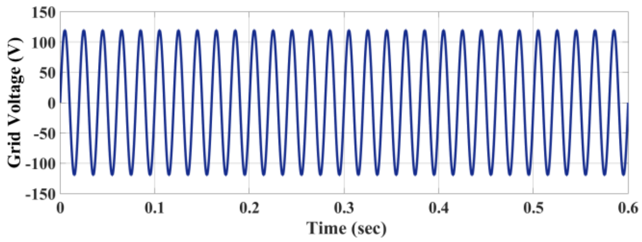


(a)

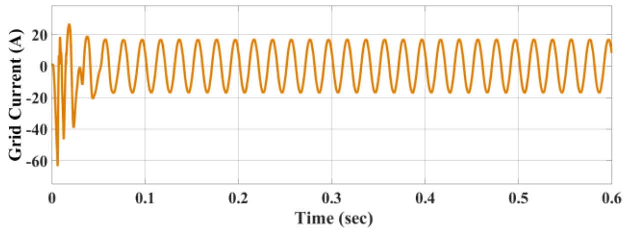


(b)

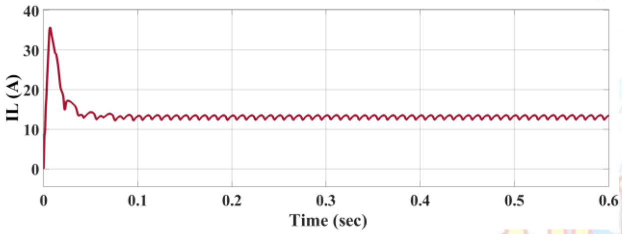


(c)

Fig. 9. Steady-state performance of the proposed ANFIS-controlled PV-based EV charging system showing (a) grid voltage, (b) grid current, and (c) DC load current (IL).

*B. Comparative Analysis of DC-Link Voltage Regulation*

Fig. 10 compares the DC-link voltage responses obtained using the conventional PI controller, CDO-optimized controller, and the proposed ANFIS controller. The PI controller exhibits a large overshoot of approximately 400 V with noticeable oscillations and a longer settling time. The CDO controller significantly reduces the overshoot and improves the transient response compared with the PI controller. The proposed ANFIS controller achieves the fastest settling time, minimum overshoot, and excellent steady-state voltage regulation around 300 V, demonstrating superior dynamic performance and robustness under transient operating conditions.

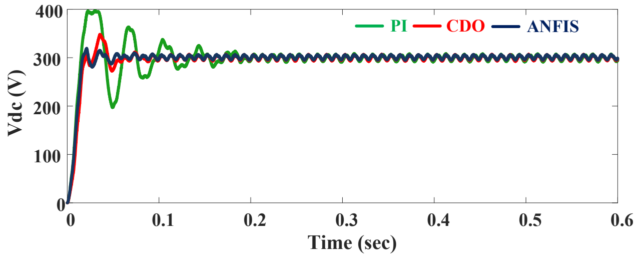


Fig.10 Simulation Results of Comparative Performance Analysis of DC-Link Voltage (Vdc) Regulation

C. Performance Analysis of the Photovoltaic (PV) System

Fig. 11 illustrates the steady-state performance of the photovoltaic (PV) system in terms of the PV voltage, PV current, and PV output power. As shown in Fig. 11(a), the PV voltage rapidly increases during the startup period and stabilizes at approximately 180 V with negligible steady-state ripple, indicating effective voltage regulation by the proposed ANFIS-controlled SEPIC–Cuk converter. The corresponding PV current shown in Fig. 11(b) exhibits an initial transient with a peak value of approximately 36 A and gradually settles to nearly 13 A, demonstrating stable current extraction from the PV array under continuous operating conditions. The PV output power illustrated in Fig. 11(c) initially reaches a peak value of about 4 kW during system startup and subsequently settles around 2.3 kW with small oscillations. The stable voltage, current, and power responses confirm that the proposed control strategy effectively extracts the available solar power while maintaining reliable converter operation and stable energy transfer to the EV charging system under varying operating conditions.

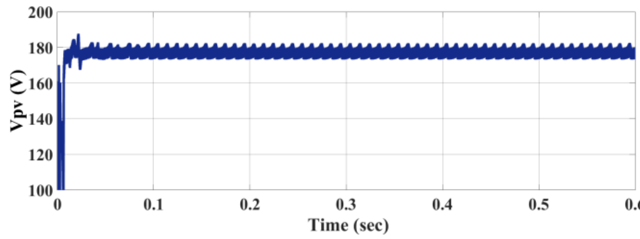


(a)

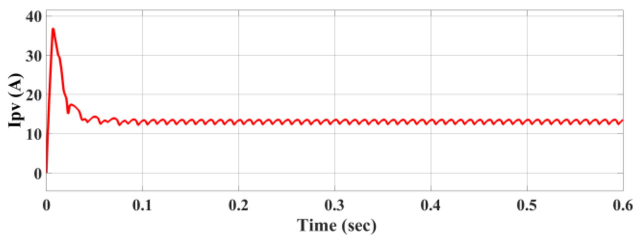


(b)

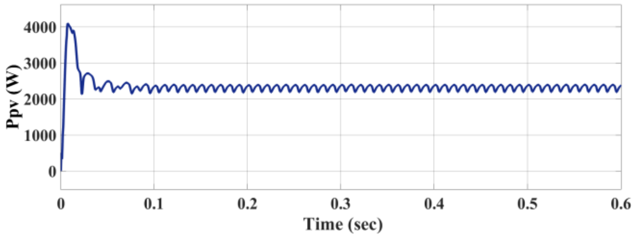


(c)

Fig. 14. Steady-state performance of the photovoltaic (PV) system showing (a) PV voltage (Vpv), (b) PV current (Ipv), and (c) PV output power (Ppv).

D. Harmonic Analysis and THD Performance Comparison

Fig. 15 compares the Fast Fourier Transform (FFT) analysis of the grid current obtained using the CDOA and proposed ANFIS controllers. As shown in Fig. 15(a), the CDOA-controlled system achieves a Total Harmonic Distortion (THD) of 2.42%, which satisfies the IEEE Std. 519 harmonic limit. However, noticeable low-order harmonic components are still present in the current spectrum. In contrast, the proposed ANFIS controller, shown in Fig. 15(b), further suppresses the harmonic components and reduces the THD to 1.84%. The reduction in harmonic distortion demonstrates the superior learning capability and adaptive control performance of the ANFIS controller under dynamic operating conditions. Consequently, the proposed ANFIS-based EV charging system provides improved grid current quality, enhanced power quality, lower harmonic distortion, and better compliance with IEEE Std. 519 compared with the CDOA-based controller.

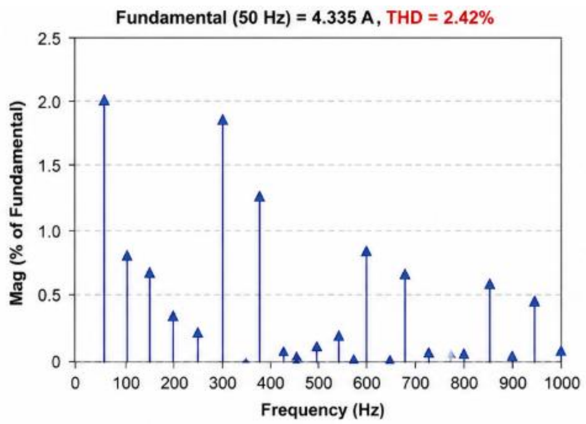


(a)

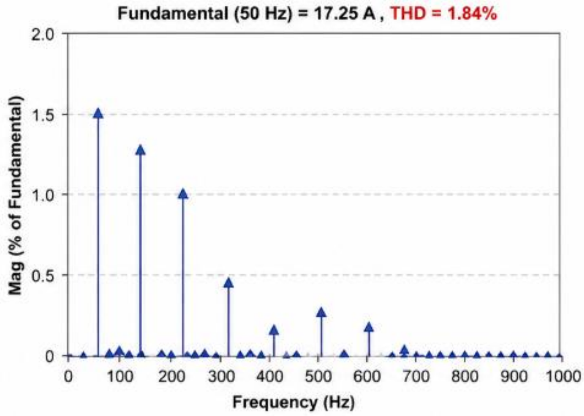


(b)

Fig. 15. Comparison of grid current harmonic spectra using (a) CDOA controller and (b) proposed ANFIS controller.

## X. CONCLUSION

This paper presented an ANFIS-controlled grid-integrated photovoltaic (PV)-based electric vehicle (EV) charging system employing a SEPIC–Cuk DC–DC converter and a grid-side Voltage Source Inverter (VSI) operating as a Shunt Active Power Filter (SAPF) for enhanced power quality and system stability. The proposed ANFIS controller effectively regulated the DC-link voltage, managed power flow between the PV array, battery energy storage system, and utility grid, and ensured stable operation under varying irradiance and load conditions. The SEPIC–Cuk converter provided high voltage gain and efficient energy conversion, while the bidirectional DC–DC converter enabled reliable battery charging and discharging. Furthermore, the SAPF successfully compensated harmonic currents and reactive power, resulting in sinusoidal grid current and improved power factor. Simulation results obtained in MATLAB/Simulink demonstrated stable PV and grid performance, faster dynamic response, improved DC-link voltage regulation, and efficient energy management. Comparative analysis showed that the proposed ANFIS controller achieved a lower grid current THD of 1.84% compared with 2.42% using the CDOA controller, thereby satisfying the IEEE Std. 519 harmonic limits. Overall, the proposed intelligent control strategy significantly improves converter performance, renewable energy utilization, EV charging efficiency, and grid power quality, making it a promising solution for future renewable energy-based smart EV charging systems.

## Conflict of interest statement

Authors declare that they do not have any conflict of interest.

## REFERENCES


[1] International Energy Agency (IEA), Global EV Outlook 2024, Paris, France, 2024.

[2] B. Singh, B. N. Singh, A. Chandra, K. Al-Haddad, A. Pandey, and D. P. Kothari, "A review of active filters for power quality improvement," IEEE Trans. Ind. Electron., vol. 46, no. 5, pp. 960–971, Oct. 1999.

[3] N. Mohan, T. M. Undeland, and W. P. Robbins, Power Electronics: Converters, Applications and Design, 3rd ed. Hoboken, NJ, USA: Wiley, 2003.

[4] H. Abu-Rub, M. Malinowski, and K. Al-Haddad, Power Electronics for Renewable Energy Systems. Wiley, 2014.

[5] T. Esram and P. L. Chapman, "Comparison of photovoltaic array maximum power point tracking techniques," IEEE Trans. Energy Convers., vol. 22, no. 2, pp. 439–449, Jun. 2007.

[6] J. A. Gow and C. D. Manning, "Development of a photovoltaic array model," IEE Proc. Electr. Power Appl., vol. 146, no. 2, pp. 193–200, Mar. 1999.

[7] N. Femia, G. Petrone, G. Spagnuolo, and M. Vitelli, Power Electronics and Control Techniques for Maximum Energy Harvesting in Photovoltaic Systems. CRC Press, 2012.

[8] F. Blaabjerg, Y. Yang, D. Yang, and X. Wang, "Distributed power-generation systems and protection," Proc. IEEE, vol. 105, no. 7, pp. 1311–1331, Jul. 2017.

[9] R. W. Erickson and D. Maksimović, Fundamentals of Power Electronics, 2nd ed. Springer, 2001.

[10] M. H. Rashid, Power Electronics Handbook, 4th ed. Butterworth-Heinemann, 2018.

[11] D. Maksimovic and S. Cuk, "Switching converters with wide DC conversion range," IEEE Trans. Power Electron., vol. 6, no. 1, pp. 151–157, Jan. 1991.

[12] K. J. Åström and T. Hägglund, PID Controllers: Theory, Design and Tuning, 2nd ed. ISA, 1995.

[13] B. K. Bose, Modern Power Electronics and AC Drives. Prentice Hall, 2002.

[14] J. S. R. Jang, "ANFIS: Adaptive-network-based fuzzy inference system," IEEE Trans. Syst., Man, Cybern., vol. 23, no. 3, pp. 665–685, May–Jun. 1993.

[15] L. A. Zadeh, "Fuzzy sets," Information and Control, vol. 8, no. 3, pp. 338–353, 1965.

[16] S. Haykin, Neural Networks and Learning Machines, 3rd ed. Pearson, 2009.

[17] C. C. Lee, "Fuzzy logic in control systems: Fuzzy logic controller," IEEE Trans. Syst., Man, Cybern., vol. 20, no. 2, pp. 404–418, Mar.–Apr. 1990.

[18] . Yen and R. Langari, Fuzzy Logic: Intelligence, Control, and Information. Prentice Hall, 1999.

[19] H. Akagi, "Active harmonic filters," Proc. IEEE, vol. 93, no. 12, pp. 2128–2141, Dec. 2005.

[20] B. Singh and K. Al-Haddad, Power Quality: Problems and Mitigation Techniques. Wiley, 2015.

[21] IEEE Recommended Practice and Requirements for Harmonic Control in Electric Power Systems, IEEE Std. 519-2022, 2022.

[22] H. Akagi, E. H. Watanabe, and M. Aredes, Instantaneous Power Theory and Applications to Power Conditioning. Wiley, 2017.

[23] M. Aredes, J. Hafner, and K. Heumann, "Three-phase four-wire shunt active filter control strategies," IEEE Trans. Power Electron., vol. 12, no. 2, pp. 311–318, Mar. 1997.

[24] B. Singh, A. Chandra, and K. Al-Haddad, Power Quality: Problems and Mitigation Techniques. Wiley, 2015.

[25] V. Khadkikar, "Enhancing electric power quality using UPQC," IEEE Trans. Power Electron., vol. 27, no. 5, pp. 2284–2297, May 2012.

[26] A. Ghosh and G. Ledwich, Power Quality Enhancement Using Custom Power Devices. Springer, 2012.

[27] Y. Yang, F. Blaabjerg, and H. Wang, "Low-voltage ride-through of grid-connected photovoltaic inverters," IEEE Trans. Ind. Appl., vol. 50, no. 3, pp. 1942–1952, May/Jun. 2014.

[28] M. Ehsani, Y. Gao, S. Longo, and K. Ebrahimi, Modern Electric, Hybrid Electric, and Fuel Cell Vehicles, 3rd ed. CRC Press, 2018.

[29] A. Emadi, Advanced Electric Drive Vehicles. CRC Press, 2014.

[30] F. Blaabjerg, M. Liserre, and K. Ma, "Power electronics converters for wind turbine systems," IEEE Trans. Ind. Appl., vol. 48, no. 2, pp. 708–719, Mar./Apr. 2012.